We are IntechOpen,
the world's leading publisher of
Open Access books
Built by scientists, for scientists

6,900
Open access books available

185,000
International authors and editors

200M
Downloads

Our authors are among the

154
Countries delivered to

TOP 1%
most cited scientists

12.2%
Contributors from top 500 universities

CLARIVATE ANALYTICS
BOOK CITATION INDEX
INDEXED

WEB OF SCIENCE™

Selection of our books indexed in the Book Citation Index
in Web of Science™ Core Collection (BKCI)

Interested in publishing with us?
Contact book.department@intechopen.com

Ferrite-Based Nanoparticles Synthesized from Natural Iron Sand as the Fe^{3+} Ion Source

Malik Anjelh Baqiya, Retno Asih, Muhammad Ghufron,
Mastuki, Dwi Yuli Retnowati, Triwikantoro
and Darminto

Abstract

Ferrite-based nanoparticles, namely, bismuth ferrite (BiFeO$_3$) and calcium ferrite (CaFe$_4$O$_7$), have been synthesized via sol-gel and chemically dissolved method, respectively, employing hematite (α-Fe$_2$O$_3$) as the Fe^{3+} ion source. Firstly, α-Fe$_2$O$_3$ nanoparticles were prepared from natural iron sand containing mostly magnetite (Fe$_3$O$_4$) phase through coprecipitation technique continued by sintering process at 800°C for 2 h. Higher BiFeO$_3$ phase content was achieved after Bi-Fe gel being annealed at 650°C for 1 h in air atmosphere. Furthermore, major phase of CaFe$_4$O$_7$ was formed with molar ratio of Fe^{3+}/Ca^{2+} = 6 and sintering temperature of 800°C for 3 h. Interestingly, the powders with dominant CaFe$_4$O$_7$ phase, known as calcium biferrite, exhibit higher ferromagnetism at room temperature. The magnetic properties of the calcium biferrite are comparable to those of barium hexaferrite which can be applied for radar-absorbing material. Meanwhile, BiFeO$_3$ powders also show weak room temperature ferromagnetism. It has also demonstrated that Ni doping in the bismuth ferrite (BiFe$_{1-x}$Ni$_x$O$_3$ with x = 0.1) nanoparticles results in enhancement of the magnetic properties. Moreover, a ferroelectric hysteresis loop and a trend of frequency dependence of the dielectric constant have been observed, which were enhanced by Pb doping (Bi$_{1-y}$Pb$_y$FeO$_3$ with y = 0.1). These results suggest a multiferroic behavior in the BiFeO$_3$ nanoparticles.

Keywords: bismuth ferrite, calcium ferrite, iron sand, multiferroic, nanoparticles, precipitation, sol-gel

1. Introduction

Development of functional nanomaterials for scientific and industrial applications is very crucial for advanced technologies. The use of natural resources as the starting compounds for producing nanomaterials is currently developing. Many researchers are exploring natural materials and even waste biomass applied as a functional material that has a high selling value for various specific applications. For example, the use of silica sand from Tanah Laut, Kalimantan, Indonesia, as a raw material for manufacturing pure SiO$_2$, zircon, and zirconia with high phase purity and crystallite size in nanometer range was reported [1]. Moreover, natural

iron sand exploration as a starting material has been shown to produce magnetite (Fe_3O_4) nanoparticles as magnetic coating, magnetic fluid (ferrofluid), and magnetic gel (ferrogel) for radar-absorbing materials, biomedical applications, and tissue engineering, respectively [2–5].

Fe_3O_4 is one of the magnetic particles that can be obtained from natural iron sand after conducting the separation technique from its impurities by mechanical and chemical processes. In nature, iron sand consists of more than 90 wt% of Fe_3O_4 particles. Generally, Fe_3O_4 has been synthesized using commercial raw materials, such as $FeCl_2.4H_2O$ and $FeCl_3.6H_2O$ [6]. The commonly used synthesis methods are sol-gel, hydrothermal, and coprecipitation techniques [7–9]. Because Fe_3O_4 nanoparticles tend to agglomerate among particles, the addition of surfactants or templates has been widely applied to produce homogeneous nanoparticles with certain sizes and morphologies [10–14]. Research on preparing Fe_3O_4 nanoparticles from iron sand has been the main topic for the past few years. The use of doping, for example, doping Mn and Zn, on Fe_3O_4 makes it superparamagnetic so that it can be applied in biomedicine applications [15–18].

Hematite (α-Fe_2O_3) is the most stable iron oxides at high temperatures. α-Fe_2O_3 is commonly obtained from iron rust which is one of the dominant corrosion products of iron metal or iron alloys. In general, α-Fe_2O_3 nanoparticles have been successfully prepared by several methods, namely, hydrothermal [19] and coprecipitation technique [20], using commercial raw materials, such as $Fe(NO_3)_3 \cdot 9H_2O$ and $FeCl_3.6H_2O$, respectively. It is found that the concentration of Fe^{3+} ions used in the preparation of α-Fe_2O_3 nanoparticles may influence the particle size and morphology, as well as the optical bandgap [20]. α-Fe_2O_3 nanoparticles with particle size of 8 nm possess superparamagnetic properties with relatively high magnetization at room temperature [21]. Therefore, it is possible to be applied for biomedical and spintronic applications. Moreover, Liu et al. have successfully prepared porous Fe_2O_3 nanorods with particle size of ~10 nm and pore sizes in the range of 5–50 nm. These porous Fe_2O_3 nanorods exhibit excellent photocatalytic properties [22].

In the field of environmental engineering, α-Fe_2O_3 nanoparticles can be synthesized from hydrated ferric chloride and ferrous sulfate salt solution through chemical coprecipitation method and calcination process at relatively high temperature of 500°C [23]. In addition, a simple chemically coprecipitation method has been employed to obtain Fe_3O_4 nanoparticles using HCl and NH_4OH as dissolving and precipitating agent, respectively [3]. Some researchers have investigated the transformation from Fe_3O_4 to α-Fe_2O_3 phase through oxidation process of Fe^{2+} to Fe^{3+} ions [24]. It is noted that Fe_3O_4 nanoparticles could be transformed into maghemite (γ-Fe_2O_3) and hematite (α-Fe_2O_3) via dry oxidation process at temperature range between 350 and 400°C and 600 and 800°C, respectively [25]. Focusing on the use of natural resources as raw materials for synthesizing functional materials, in this chapter, α-Fe_2O_3 nanoparticles were synthesized from natural iron sand through chemical coprecipitation method followed by sintering process at temperature of 800°C. Then, the obtained α-Fe_2O_3 nanoparticles were utilized as one of the raw materials for preparing calcium ferrite (Ca-ferrites) and bismuth ferrite ($BiFeO_3$) nanoparticles as potential materials for radar-absorbing and data storage materials, respectively. The physical characterizations for all obtained ferrite-based nanoparticles include elemental and phase identification, particle morphology, and magnetic and electrical properties.

Based on the phase diagram of CaO-Fe_2O_3 system [26, 27], it is known that there are three main phases of calcium ferrite compounds and those are $2CaO.Fe_2O_3$ ($Ca_2Fe_2O_5$), $CaO.Fe_2O_3$ ($CaFe_2O_4$), and $CaO.2Fe_2O_3$ ($CaFe_4O_7$). It is possible that the reaction between CaO and Fe_2O_3 results in other unstable calcium ferrite phases, such as $CaFe_{12}O_{19}$. In addition, Boyanov [28] has pointed out that the mixture of

$CaCO_3$-Fe_2O_3 after thermal treatment has produced various types of calcium ferrite compounds consisting of ~50% $CaO.2Fe_2O_3$, ~20% $CaO.Fe_2O_3$, ~8% $2CaO.Fe_2O_3$, and other ferrite products. The formation of calcium ferrite compounds depends on the kinetics of chemical reaction at the boundary between the phases and oxide diffusion during the reaction affected by the concentration ratio of the existing Ca^{2+} and Fe^{3+} ions as the precursors and also the atmospheric condition [29].

Calcium ferrite compounds exhibit soft ferromagnetism, and, therefore, it can be used for radar-absorbing materials in the calcium ferrite/graphite nanocomposites [30]. In this case, calcium ferrite nanoparticles have magnetic properties that are comparable to barium ferrite ($BaO.6Fe_2O_3$) and strontium ferrite ($SrO.6Fe_2O_3$) known as M-type hexaferrite for microwave-absorbing applications. In order to be used for this application and also for biomedical applications as targeted drug delivery, calcium ferrite should exhibit superparamagnetic behavior [31]. Compared with the other ferrites, such as MFe_2O_4 (M = Zn, Mn, Ni, and Cu), $CaFe_2O_4$ is one of the biocompatible materials and environmentally friendly due to the use of calcium rather than heavy metals. Moreover, $Ca_2Fe_2O_5$ with the brownmillerite structure has a specific application as p-type thermoelectric device [32]. This is due to the fact that this compound has interesting electrical properties [33, 34]. Oxygen deficiencies in the $Ca_2Fe_2O_5$ crystals may enhance the electrochemical activity [35]. On the other hand, $CaFe_4O_7$ has not been explored yet regarding its magnetic properties. In contrast to the other calcium ferrites, in this chapter, $CaFe_4O_7$ nanoparticles were prepared by mixing Fe_2O_3 from natural iron sand and $CaCO_3$ from natural limestone.

Bismuth ferrite ($BiFeO_3$) is one of multiferroic system showing a magnetic-electric coupling at room temperature. Multiferroic material has perovskite structure with chemical formula ABO_3. The type of A and B sites, the cation nonstoichiometry, and the presence of oxygen vacancies may have an impact on the structural, electronic, and magnetic properties [36]. $BiFeO_3$ crystallizes in a distorted rhombohedral perovskite with space group R3c [37]. It has high Curie temperature and Néel temperature of 1100 and 640 K, respectively [38]. It is difficult to obtain a pure phase of $BiFeO_3$ because the kinetics of phase formation leads to the formation of secondary phases, such as $Bi_{25}FeO_{40}$ (sillenite) and $Bi_2Fe_4O_9$ (mullite). Various techniques have been reported to prepare single phase of $BiFeO_3$, and those are chemical coprecipitation [39], hydrothermal [40], and sol-gel methods [41–43]. The ideas of those techniques are to achieve a single phase of $BiFeO_3$ with a simple route, low temperature, and cost-effectiveness. Wang et al. have found that the formation of $BiFeO_3$ phase starts at 425°C with impurity phases about 30% by the low-heating temperature solid-state precursor method [44, 45]. Further calcination from 450 to 550°C results in a pure $BiFeO_3$ phase without any impurity phases. However, impurity phase of $Bi_2Fe_4O_9$ has been detected in the powder calcined at above 650°C. Moreover, $BiFeO_3$ nanoparticles synthesized by microwave-assisted sol-gel method at calcination temperature of 450°C exhibit a pure phase of $BiFeO_3$ structure with particle size of 40 nm and no detected secondary phase [46].

Magnetic and dielectric properties of $BiFeO_3$ nanoparticles are determined by the introduction of doping and particle size influenced by the synthesis method, temperature, and duration of calcination. It has been found that all magnetic parameters, such as saturation magnetization, enhance with decreasing particle size [43]. $BiFeO_3$ nanoparticles with the size below 100 nm have weak ferromagnetism at room temperature. This ferromagnetic behavior in the nanoparticles is due to the presence of oxygen vacancies in $BiFeO_3$ system [41, 47]. Enhancement of magnetic as well as dielectric properties in $BiFeO_3$ can be achieved by adding doping of Mn, Ni, Pb, Ti, Sr, and Zn [48–56]. Up to the present, there have been various studies examining the doping effects of $BiFeO_3$ nanoparticles with numerous advanced

techniques to improve their performance. In the case of the enhancing magnetization-induced by doping, it has been suggested that this is probably due to increasing distortion of local structure, increasing the effect of Dzyaloshinskii-Moriya (DM) interaction, distortion of Fe and O bonding, destruction of spin cycloid structure, and the presence of impurity phase in the $BiFeO_3$ systems [53, 57]. Besides affecting the magnetic properties, introduction of doping in $BiFeO_3$ leads to the improvement of dielectric and ferroelectric properties [50, 58, 59]. Yuan et al. [54] have found that a sufficient amount of Sr/Pb doping can improve the magnetic properties as well as high-frequency dielectric properties.

In addition, the dielectric properties of pure $BiFeO_3$ phase strongly depend on the atmospheric condition during the powder synthesis. Liu et al. [60] have found a higher spontaneous polarization and lower breakdown field based on polarization-electrical field (P-E) hysteresis loops in the samples annealed in H_2 and N_2 atmospheres. In this chapter, $BiFeO_3$ nanoparticles were synthesized by sol-gel method using natural iron sand as one of the raw materials and calcined in air atmosphere. Then, the ferroelectric and the dielectric properties were intensively investigated in the Pb- and Ni-doped $BiFeO_3$ nanoparticles.

2. Preparation of hematite (α-Fe_2O_3) nanoparticles

Prior to the preparation of α-Fe_2O_3 nanoparticles, at first, Fe_3O_4 nanoparticles were synthesized from natural iron sand as the raw material by coprecipitation technique using HCl as dissolving agent and NH_4OH as precipitating agent. The detail of experimental procedure to synthesize Fe_3O_4 nanoparticles was also described in elsewhere [3]. First of all, the extracted iron sand was collected and dissolved in 12 M HCl at ~70°C under continuous and constant stirring of 600 rpm. The obtained solution from the reaction process was filtered and added slowly with 6.49 M NH_4OH under the same temperature and stirring speed for 30 minutes. Then, the black precipitates were formed. The precipitate (Fe_3O_4 phase) was initially washed with distilled water until pH 7 and then dried at 70°C for 5 h. In order to get α-Fe_2O_3 phase, the dried nanopowder (Fe_3O_4 phase) was calcined at 800°C for 2 h, as shown in **Figure 1**. Finally, the Fe_2O_3 powders from this calcination were continued by performing coprecipitation process again with the same experimental procedure as before until the precipitation process. A reddish
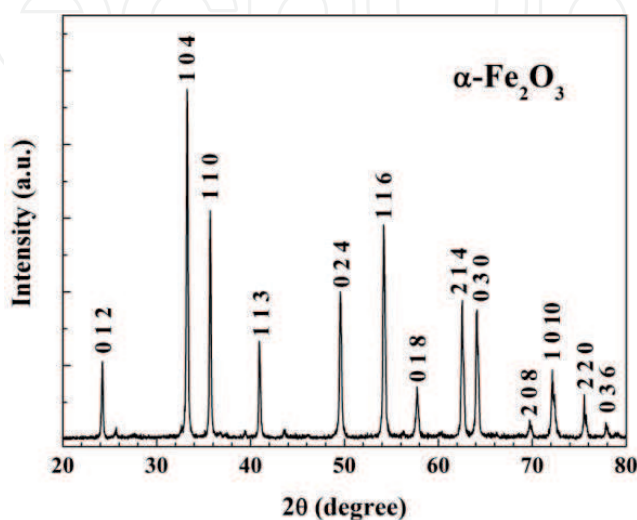

Figure 1.
Hematite (α-Fe_2O_3) synthesized from natural iron sand (Fe_3O_4) by coprecipitation method followed by calcination process at 800°C for 2 h.

precipitate ($Fe_2O_3.H_2O$) was formed. The resulted precipitate was then washed and collected for further synthesis of $CaFe_4O_7$ and $BiFeO_3$ (without and with doping of Pb and Ni) nanoparticles.

3. Preparation of calcium ferrite nanoparticles

Calcium biferrite ($CaFe_4O_7$) nanoparticles were synthesized by the so-called chemically dissolved method using precipitated $CaCO_3$ and Fe_2O_3 as Ca^{2+} and Fe^{3+} ion sources, respectively. Fe_2O_3 powders were obtained as described previously from natural iron sand, whereas the precipitated $CaCO_3$ particles were synthesized from natural limestone through carbonation process. First, the natural limestone was extracted from the existing impurities, such as silica, and then it was calcined at 900°C for 6 h to produce CaO. The CaO powder was dissolved into distilled water to produce $Ca(OH)_2$ solution. The carbonation process using CO_2 gas flow was performed until it formed a precipitation at pH around 7. The precipitated $CaCO_3$ was filtered and dried for further synthesis. The detail procedure was also explained in the former paper by Arifin et al. [61].

In the synthesis of the calcium ferrite nanoparticles using the chemically dissolved method, the obtained Fe_2O_3 and precipitated $CaCO_3$ were dissolved in HNO_3 to get $Fe(NO)_3$ and $Ca(NO)_2$ solutions, respectively, with a molar ratio of 1:6. Both solutions were mixed homogeneously and heated at constant temperature (80°C) and stirring rate (600 rpm) until it formed slurry precipitates. The precipitates were washed using distilled water and dried at 80°C for 10 h. The resulted powders were collected and then sintered at 800°C for 3 h.

4. Preparation of bismuth ferrite ($BiFeO_3$) nanoparticles without and with Pb and Ni doping

Nanoparticles of undoped, Pb- and Ni-doped $BiFeO_3$ ($BiFeO_3$, $Bi_{0.9}Pb_{0.1}FeO_3$, and $BiFe_{0.9}Ni_{0.1}O_3$, respectively) were prepared by sol-gel method. The starting materials were Fe_2O_3 synthesized previously from iron sand (94%) as the Fe^{3+} ion source and Bi_2O_3 (Aldrich, 99.9%) as the Bi^{3+} ion source. $Pb(NO_3)_2$ (powder, 99%) and $Ni(NO_3)_2.6H_2O$ (powder, 99%) were used as the Pb and Ni doping, respectively. Fe_2O_3, Bi_2O_3, $Pb(NO_3)_2$, and $Ni(NO_3)_2.6H_2O$ powders were dissolved separately by HNO_3 (Merck, 65%) to form solutions of ferrite nitrate, bismuth nitrate, lead nitrate, and nickel nitrate, respectively, with the stoichiometric molar ratio of (Bi, Pb):(Fe, Ni) = 1:1. Acetic acid was added into each solution under constant stirring and temperature for 30 minutes. Then, it was followed by addition of ethylene glycol under the same condition. Next, the obtained solutions were mixed together under the same temperature and stirring rate for 1 h. The resulted solution was dried at 80°C for 6 days to obtain the undoped and doped $BiFeO_3$ xerogels. The dried gels were ground and collected. Finally, the powders were calcined in air at 650 and 700°C for 1 h to form undoped $BiFeO_3$ and doped $BiFeO_3$ ($Bi_{0.9}Pb_{0.1}FeO_3$ and $BiFe_{0.9}Ni_{0.1}O_3$), respectively, for further characterizations.

5. Characterizations

A thermogravimetric/differential thermal analysis (TG/DTA) was performed to determine the thermal behaviors of the dried gel of bismuth ferrite. The phase formation and crystal structure of all samples were characterized by X-ray

diffraction (XRD) with Cu-K$_\alpha$ radiation and λ = 1.54056 Å for scanning 2θ range of 20–70°. The lattice parameters and average crystallite sizes were determined by XRD patterns which were analyzed by the Rietveld method using the Rietica and MAUD programs [62, 63]. Transmission electron microscopy (TEM) with selected area electron diffraction (SAED) pattern was conducted to investigate the particles' morphology and crystal structure confirmation of all ferrite-based samples. The magnetic properties of the nanoparticles were measured using vibrating sample magnetometry (VSM, Oxford VSM1.2H) and superconducting quantum interference device (SQUID) magnetometer in external magnetic field range of ±1 T at room temperature. The ferroelectric properties of the bismuth ferrites were studied from the polarization-electric field (P-E) hysteresis loops using a polarization meter (Radiant Technologies 66A). Frequency dependence of the dielectric constant of all bismuth ferrites was estimated by two-probe electrical resistance using Automatic RCL Meter (type PM6303A).

6. Structural and magnetic properties of calcium ferrites from natural iron sand and limestone

Figure 2 shows the XRD pattern of calcium ferrite compound synthesized by the chemically dissolved method from natural iron sand and limestone as the raw materials and then sintered at 800°C for 3 h. Based on the analysis of phase identification, it can be seen that the resulted powder contains several phases of calcium ferrites, $CaFe_4O_7$, $Ca_4Fe_{14}O_{25}$, and $Ca_2Fe_9O_{13}$, with weight percentages of 28.8, 46.6, and 24.6 wt%, respectively. The formation of those phases is possible to occur due to the atmospheric condition during calcination. Generally, at relatively high calcination temperatures, the most stable phases are those that have higher coordination numbers, in this case with surrounding oxygen. Hughes et al. [64] have also identified these distinct calcium ferrite phases in the mixture of CaO and Fe_2O_3 calcined in air at high temperatures between 1180 and 1240°C. In addition, the phase formation of $Ca_2Fe_9O_{13}$ can be present in the compound at the lower temperatures [65]. With the increase of temperature, the phase formation becomes more complex. Related to the phase transformation, it strongly depends on the crystallization kinetics of the reaction, the ratio concentration between Ca and Fe ions, and the atmospheric condition [66].
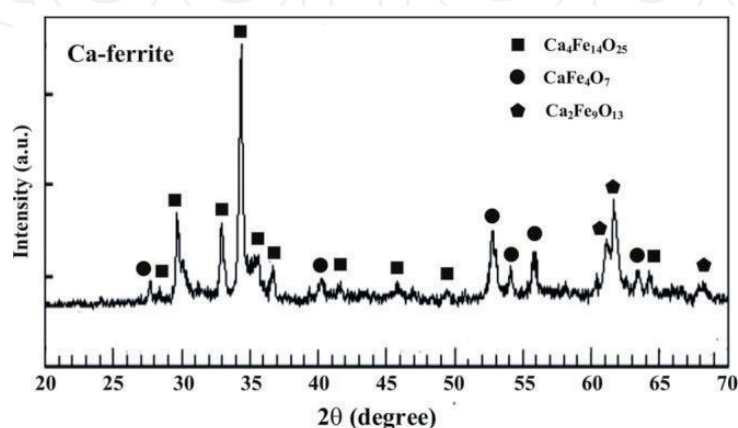

Figure 2.
XRD pattern of calcium ferrite powders synthesized by the chemically dissolved technique from natural iron sand and limestone as the Fe³⁺ and Ca²⁺ ion sources, respectively, and then continued by calcination process at 800°C for 3 h.

Focusing on the high intensities of the diffraction peaks, the sample exhibits XRD lines of both $CaFe_4O_7$ and $Ca_4Fe_{14}O_{25}$ phases as the dominant phases. $CaFe_4O_7$ has monoclinic structure and $Ca_4Fe_{14}O_{25}$ has hexagonal structure. Both phases have similar crystalline structure related to hexagonal ferrite structures [67]. The XRD pattern in **Figure 2** shows that $CaFe_4O_7$ and $Ca_4Fe_{14}O_{25}$ phases have broad diffraction peaks. This indicates that the average crystallite sizes are in a nanometer scale. Based on the Rietveld analysis, $CaFe_4O_7$ phase in the calcium ferrite compound has average crystallite size of about 46 nm. In order to clarify the nano-sized particles, TEM image is important to be investigated in detail.

Figure 3 displays TEM image of the calcium ferrite sample together with the selected area electron diffraction (SAED). The TEM image proves that the particle size of the sample is in the range of 40–60 nm. This is in a good agreement with the Rietveld analysis of the XRD pattern in **Figure 2**. The analysis of electron diffraction from SAED pattern reveals that $CaFe_4O_7$ and $Ca_4Fe_{14}O_{25}$ phases are dominantly present and $Ca_2Fe_9O_{13}$ is the minor phase in the sample. This result is also consistent with the XRD pattern analysis.

Magnetic properties of the calcium ferrite compound were studied by the magnetic hysteresis curve (M-H curve) at room temperature as shown in **Figure 4**. It is clear that the sample exhibits ferromagnetic behavior. A detailed observation on the M-H curve of the sample shows that the values of remanent magnetization and magnetization at 1 T are 2.11 and 10.94 emu/g, respectively. This indicates that a soft magnetism is realized in the calcium ferrite compound. It has been found that the dominant phase existing in the sample has a contribution to the ferromagnetic behavior [68]. The value of magnetism in the sample is comparable with that of the barium-calcium hexaferrite prepared by sol-gel and microemulsion techniques, in which the saturation magnetization value is approximately 24 emu/g [69]. Moreover, Samariya et al. [70] have studied the magnetic properties of calcium ferrite, in the form of $CaFe_2O_4$, nanoparticles. They have found similar value of magnetization compared with the present result in this work. Concerning the multiphase compound, the magnetic parameters in the sample are influenced by the presence of nonmagnetic phase, magnetic domain and its orientation, and defect formation. Therefore, it is important to investigate more detail on how to prepare a pure certain phase of calcium ferrite from natural resources as the starting materials. Accordingly, this result demonstrates that the present calcium ferrite nanoparticles could be used as one of the potential materials for microwave absorption application.
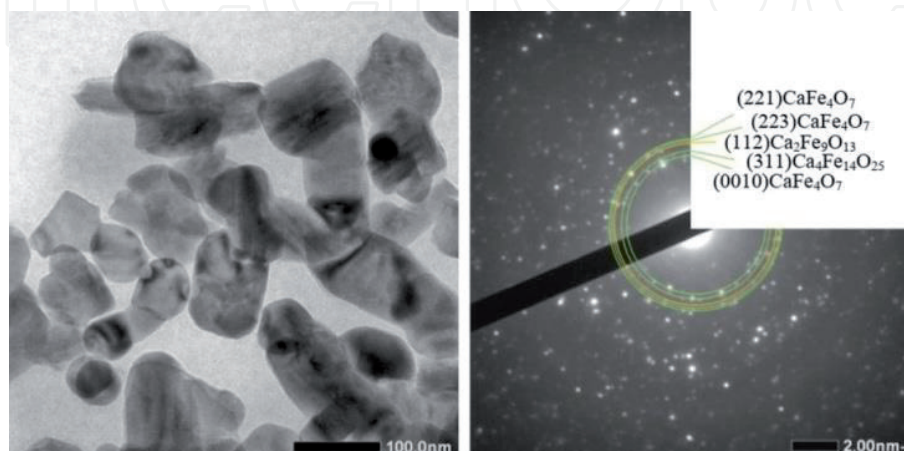

Figure 3.
TEM image with selected area electron diffraction (SAED) pattern for calcium ferrite powders synthesized by the chemically dissolved technique from natural iron sand and limestone as the Fe³⁺ and Ca²⁺ ion sources, respectively, and then continued by calcination process at 800°C for 3 h.
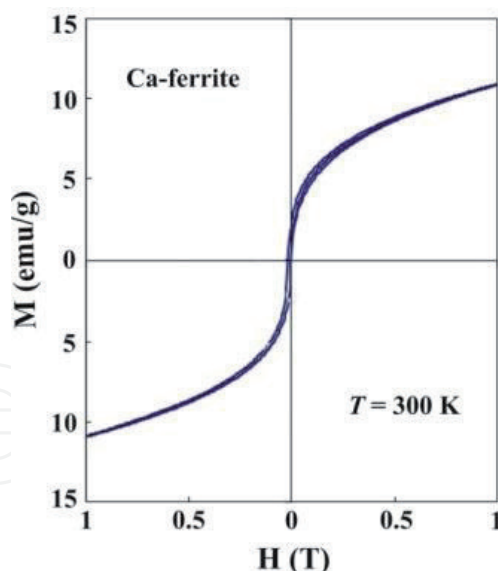
Figure 4.
Magnetization curve at room temperature for calcium ferrite powders synthesized by the chemically dissolved technique from natural iron sand and limestone as the Fe^{3+} and Ca^{2+} ion sources, respectively, and then continued by calcination process at 800°C for 3 h.

7. Magnetoelectric properties of bismuth ferrite nanoparticles

TG/DTA curve of the uncalcined powder of the undoped $BiFeO_3$, shown in **Figure 5**, exhibits about 29% weight loss from room temperature to 550°C due to the evaporation of water, organics, and nitrate decomposition [71, 72]. Based on this thermal behavior, the powder could be thermally treated at temperatures from 500 up to 700°C for 1 h. Carvalho et al. [73] have reported that the increasing time of the heat treatment increases the formation of secondary phases and, therefore, they have suggested to avoid a long heat treatment to synthesize $BiFeO_3$ nanoparticles.

Figure 6 shows the XRD patterns of the undoped and doped $BiFeO_3$ samples calcined at 650 and 700°C, respectively, for an hour in air atmosphere. This heat treatment was conducted to form $BiFeO_3$ phase. The influence of the atmosphere in the phase formation has been investigated by Xu et al. [72]. They have reported that crystallization in the atmosphere is important to obtain a pure $BiFeO_3$ phase prepared by sol-gel method. It can be seen from the phase identification of the XRD patterns that multiphases of bismuth ferrite compounds such as $BiFeO_3$, $Bi_{25}FeO_{40}$, and $Bi_2Fe_4O_9$ were observed in the synthesized powders. Moreover, Bi_2O_3 was still observed in the XRD patterns in minor composition. $BiFeO_3$ is a metastable phase which easily decomposes to secondary phases, $Bi_{25}FeO_{40}$ and $Bi_2Fe_4O_9$, at high temperatures [73]. In this present work, it is found that higher $BiFeO_3$ phase is achieved with heat treatment at 650°C for 1 h. This result is consistent with the TG/DTA and XRD data analyzed by Sakar et al. [74] which corresponds to sharp diffraction peaks of the $BiFeO_3$ phase. The formation of secondary phases increases at higher temperature than 650°C. $BiFeO_3$ began to decompose because of its unstable thermodynamic character when the calcination temperature was further increased. The relative weight percent and average crystallite size of the $BiFeO_3$ phase were determined from the diffraction patterns by Rietveld method using Rietica and MAUD program, respectively. Overall, the analysis results show that the bismuth ferrite powders contain about 75 wt% of $BiFeO_3$ phase. The average crystallite size of the $BiFeO_3$ sample prepared at 650°C is about 84 nm.

The addition of doping substituting the A and B sites in the ABO_3 perovskite structure of $BiFeO_3$ greatly affects the crystal distortion and changes in the
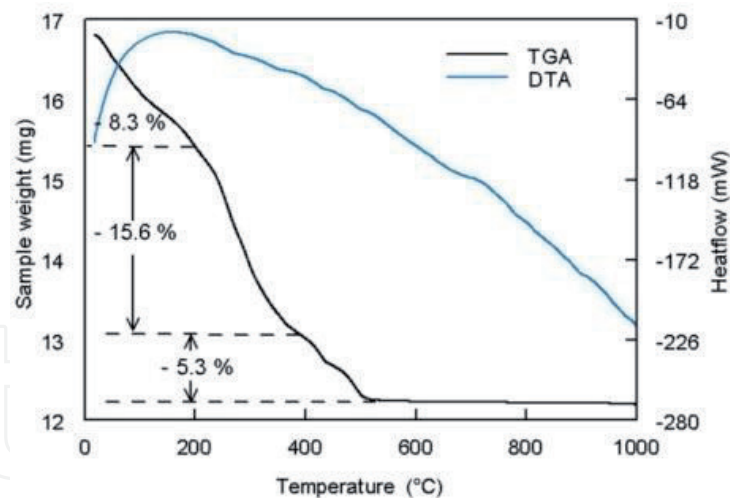
Figure 5.
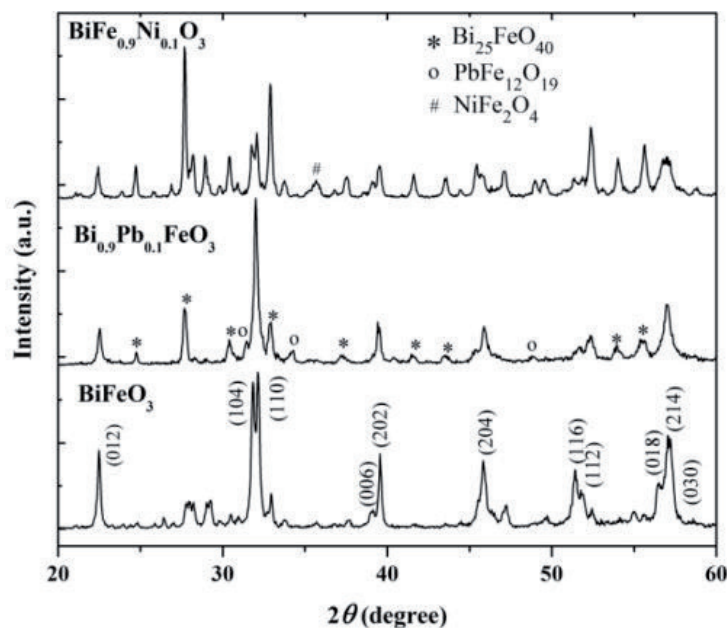*TG/DTA curves of the uncalcined $BiFeO_3$ powder.*

Figure 6.
XRD patterns of the undoped $BiFeO_3$ and doped $BiFeO_3$ ($Bi_{0.9}Pb_{0.1}FeO_3$ and $BiFe_{0.9}Ni_{0.1}O_3$) powders synthesized by sol-gel method calcined at 650 and 700°C, respectively, for 1 h in air.

composition of the secondary bismuth ferrite phases. Pb ion substitutes A site, namely, the Bi^{3+} ion, in the structure of $BiFeO_3$. As a result, Pb doping has an effect on the diffraction peak shift of the $BiFeO_3$ phase to the lower diffraction angle. This is because the ionic radius of Pb^{2+} ion (0.119 nm) is greater than that of Bi^{3+} ion (0.103 nm). Moreover, it can also be seen that there is a combination of the diffraction peaks for the crystal plane (006) and (202) into the diffraction peak (111) at 2θ of 31–32°. This indicates a small change in the distortion of the crystal from distorted rhombohedral to pseudocubic system. XRD analysis confirms that $Bi_{0.9}Pb_{0.1}FeO_3$ has cubic structure with space group of *Pm-3 m*, compared with the undoped $BiFeO_3$ having rhombohedral structure with space group of R3c. It is important to mention that the secondary phase in the Pb-doped $BiFeO_3$ ($Bi_{0.9}Pb_{0.1}FeO_3$) sample, which is $PbFe_{12}O_{19}$, has been reported to be one of the hexaferrite materials exhibiting good superparamagnetic behavior [75]. Further Rietveld analysis from the XRD patterns gives the values of lattice parameters of $BiFeO_3$, $Bi_{0.9}Pb_{0.1}FeO_3$, and $BiFe_{0.9}Ni_{0.1}O_3$ as shown in **Table 1**.

On the XRD pattern of the Ni-doped $BiFeO_3$ ($BiFe_{0.9}Ni_{0.1}O_3$) sample, shown in **Figure 6**, it is clear that there is no change of the crystal structure due to Ni doping at the B site (Fe^{3+} ion) of $BiFeO_3$ crystal. This is displayed by the rhombohedral peak which can still be observed at 2θ of 31–32°. The result of the phase composition analysis gives that there is an increase of secondary phases ($Bi_{25}FeO_{40}$) and the presence of $NiFe_2O_4$ in the sample. Interestingly, both secondary phases have also unique magnetoelectric properties. It has been reported by Zhu et al. [76] that $Bi_{25}FeO_{40}$ has good dielectric and electrical properties which can be used as one of integrated circuit components. $NiFe_2O_4$ is one of magnetic spinel structures with good magnetic and dielectric properties [77]. In addition, Ni doping in the $BiFeO_3$ system has an effect on diffraction peak shift to the lower diffraction angle because ionic radius of Ni^{3+} ion (0.069 nm) is slightly larger than that of Fe^{3+} ion (0.065 nm). The change of lattice parameter due to Pb and Ni doping in $BiFeO_3$ system is summarized in **Table 1**.

Figure 7 shows the TEM image and selected area electron diffraction (SAED) patterns of $BiFeO_3$ powders annealed at 650°C for 1 h in air. Sharp diffraction spots seen from SAED pattern confirm the formation of well crystalline bismuth ferrites. Phases identified from SAED pattern are relatively matching with the XRD patterns in **Figure 6** consisting of $BiFeO_3$, $Bi_{25}FeO_{40}$, $Bi_2Fe_4O_9$, and Bi_2O_3. The TEM image shows typical morphology of particle agglomeration. The particle size is greater than the average crystallite size estimated by Rietveld analysis due to agglomeration of the nanoparticles.

The nonlinear magnetic hysteresis curve of the bismuth ferrite powders, as shown in **Figure 8**, illustrates weak ferromagnetism. The remanent magnetization of 0.044 emu/g and coercive field of 68.5 Oe in the undoped $BiFeO_3$ confirm the weak ferromagnetism behavior at room temperature. The complete saturation of magnetization of powders was not achieved up to applied magnetic field of 1 T. The hysteresis loop of bulk $BiFeO_3$ is generally linear indicating antiferromagnetic order at the ground state (5 K) [78]. The weak ferromagnetic order of these powders can be understood as a result of residual magnetic moment caused by its canted spin structure [79]. The canting of the spins can be caused by reduction of particle size. When the particle size decreases, the number of surface asymmetry atoms increases, then it changes the angle of the helical ordered spin arrangement, and finally the net magnetic moment appears [80]. Moreover, the existence of defects, for instance, oxygen vacancies [81], and the secondary phases [82] may contribute to the weak ferromagnetic behavior.

Based on the magnetic hysteresis loops of the doped $BiFeO_3$ nanoparticles, the Pb doping in the $BiFeO_3$ structure seems to have a small effect on the magnetic properties. Substitution of Pb^{2+} ions at the Bi^{3+} sites induces oxygen vacancies which may lead to the enhancement of magnetic moments in the sample [83]. However,

Sample	Structure	Lattice parameters (Å)
$BiFeO_3$	Rhombohedral	a = b = 5.578 (1)
		c = 13.862 (3)
$Bi_{0.9}Pb_{0.1}FeO_3$	Cubic	a = b = c = 3.958 (1)
$BiFe_{0.9}Ni_{0.1}O_3$	Rhombohedral	a = b = 5.574 (1)
		c = 13.840 (4)

Table 1.
Rietveld analysis results for the XRD patterns of the undoped $BiFeO_3$ and doped $BiFeO_3$ ($Bi_{0.9}Pb_{0.1}FeO_3$ and $BiFe_{0.9}Ni_{0.1}O_3$) powders.
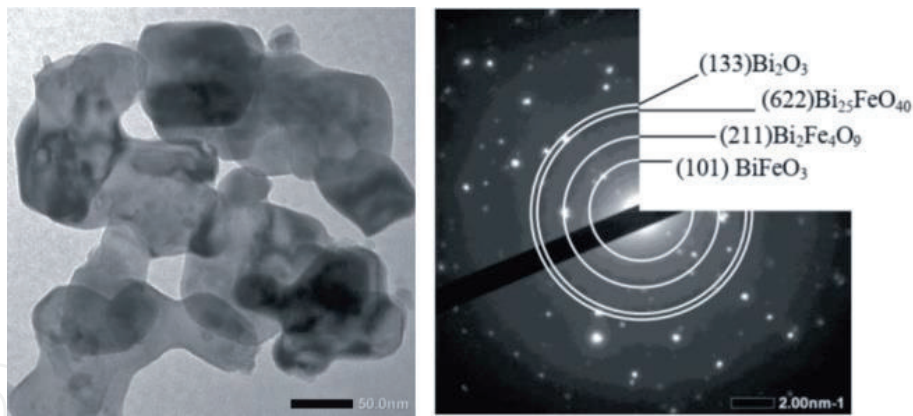
Figure 7.
TEM image with selected area electron diffraction (SAED) pattern for barium ferrite powders synthesized by sol-gel method and then calcined at 650°C for 1 h in air.
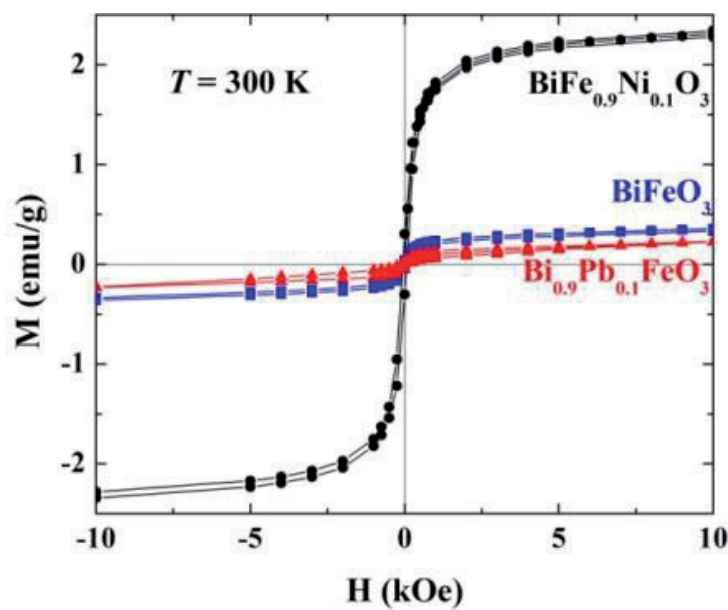

Figure 8.
Magnetic hysteresis curves of the undoped BiFeO$_3$ and doped BiFeO$_3$ (Bi$_{0.9}$Pb$_{0.1}$FeO$_3$ and BiFe$_{0.9}$Ni$_{0.1}$O$_3$) powders synthesized by the sol-gel method.

Verma and Kotnala [84] have confirmed through the SQUID measurements that BiFeO$_3$ with Pb doping exhibits a strong antiferromagnetism suggesting that the reduction of oxygen vacancies is realized in the system. Moreover, Ederer and Spaldin [85] have proposed that the magnetization value can be affected by the presence of oxygen vacancies but with a small change due to the formation of Fe^{2+} at the BiFeO$_3$ sites adjacent to the vacancy. Therefore, there is almost no increase in the magnetic parameters after Pb doping. Moreover, the weak ferromagnetism is commonly observed in the Bi$_{1-x}$A$_x$FeO$_3$ (A = Ca, Sr., Pb, Ba) system providing a canting of the antiferromagnetic sublattice [86], which is in line with this present work. On the other hand, Ni-doped BiFeO$_3$ nanoparticles show a significant increase on the magnetic parameters, namely, remanent and saturation magnetization. This result is consistent with the previous paper by Hwang et al. [87], in which the Ni-doped BiFeO$_3$ sample exhibits similar rhombohedral perovskite structure compared to that of the undoped one and the magnetic properties show enhancement with respect to the undoped one. The increase in magnetic properties can occur due to the effect of nanoparticle surface area and ferromagnetic interaction exchange between neighboring Fe^{3+} and Ni^{3+} ions in the BiFeO$_3$ system [88].

The room temperature P-E loop of the prepared undoped bismuth ferrite, presented in **Figure 9**, exhibits unsaturated hysteresis loop. The curve was not fully saturated because of the low applied electric field. The remanent polarization (R_s) and the coercive field (E_c) of the undoped $BiFeO_3$ nanoparticles are about 20.5 μC/cm^2 and 5.5 V/cm, respectively. These values are lower than the values reported in the single crystal which has a large polarization of ~100 μC/cm^2 along (111) for bulk bismuth ferrite [89]. The existence of secondary phases, such as $Bi_{25}FeO_{40}$, $Bi_2Fe_4O_9$, and Bi_2O_3, affects the lower values of R_s and E_c in the sample. Pradhan et al. [78] have reported that leakage current is one of the major reasons for obtaining lower values of saturation polarization (P_s), R_s, and E_c in $BiFeO_3$ system.

In the Pb-doped $BiFeO_3$ nanoparticles, the Pb substitution improves the dielectric and ferroelectric properties [90]. It can be seen from **Table 2** that the electric properties, including dielectric constant, electrical conductivity, and electrical permittivity, increase with Pb doping in the $BiFeO_3$ crystal. It has been found that Pb substitution on the Bi site in the $BiFeO_3$ may destroy ferroelectricity ordering induced by Bi lone pair in the rhombic structure until it reaches a stable pseudocubic structure of $BiFeO_3$ [91]. In this work, addition of Pb doping in $BiFeO_3$ with x = 0.1 has already resulted in a pseudocubic structure, and, hence, the enhancement of the electrical properties is realized in the present sample. The value of dielectric constant with Pb doping, x = 0.1, at 1 kHz is in a good agreement with the work done by Zhang et al. [92]. The defect of oxygen vacancy due to Pb doping can increase the polarity of the sample and finally increase its dielectric constant. In addition, oxygen vacancy created as the consequence of Pb substitution on Bi site in the $BiFeO_3$ system plays an important role related to the ferroelectricity for Pb-doped $BiFeO_3$ sample. Moreover, the presence of Pb doping causes the existence of Fe^{2+} ion at Fe^{3+} sites which can produce holes around the Fe^{3+} site [93]. This effect is shown by the increasing value of electrical conductivity. It has been suggested that the relatively low number of oxygen vacancies in this sample may result in an improvement of the ferroelectric properties [94], as shown in **Table 2**.

As mentioned earlier, the Ni doping in $BiFeO_3$ nanoparticles enhances the magnetic properties as reported in the former paper [88]. However, the dielectric and
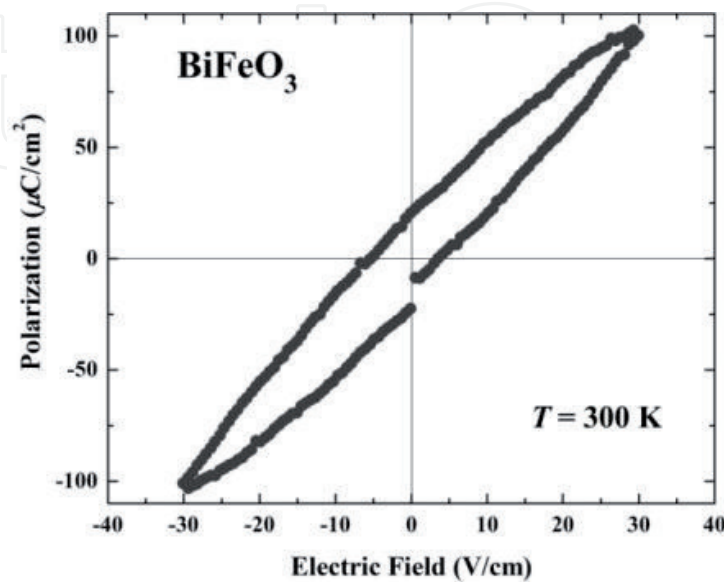

Figure 9.
Room temperature polarization-electric field (P-E) hysteresis loop of the undoped $BiFeO_3$ pellet sintered at 750°C.

Sample	Dielectric constant (ε_r) $f = 1\,kHz$, $T = 300\,K$	Conductivity $[\times 10^{-4}\ (\Omega\,m)^{-1}]$ $T = 300\,K$	Permittivity ($\times 10^{-10}\ F/m$) $T = 300\,K$
$BiFeO_3$	19.4	0.012	1.7
$Bi_{0.9}Pb_{0.1}FeO_3$	130.8	0.162	11.6
$BiFe_{0.9}Ni_{0.1}O_3$	17.5	0.010	1.6

Table 2.
Dielectric constant, electrical conductivity, and permittivity of the undoped $BiFeO_3$ and doped $BiFeO_3$ ($Bi_{0.9}Pb_{0.1}FeO_3$ and $BiFe_{0.9}Ni_{0.1}O_3$) powders measured at room temperature.

other electrical properties of the Ni-doped $BiFeO_3$ have lower values than those of the undoped one, as displayed in **Table 2**. This means that the sample has inappropriate Ni doping concentration to improve the ferroelectricity. Moreover, the reduction in the dielectric constant is attributed to the decrease in the total polarization occurring in the sample. It is well known that the total polarization of a dielectric material is a combination of electronic, ionic, dipolar, and interfacial/space charge polarizations. The lower value of dielectric constant is probably caused by the effect of Ni doping on the ionic transformation from Fe^{2+} to be Fe^{3+} again. As the consequence of the charge stability, it may consume holes. Hence, the holes as charge carrier decrease. This is one reason of the decrease of sample's conductivity [95]. Another possible reason on decreasing value of electrical properties in Ni-doped $BiFeO_3$ sample is the impurity effect. It should be noticed that the impurity phases such as $Bi_2Fe_4O_9$ and $Bi_{25}FeO_{40}$ may also contribute to the electrical properties in $BiFeO_3$ [48]. The existence of multiphase in the sample leads to the increase of insulating grain boundaries affecting the electrical conductivity as well as the total polarization in the sample. The increase in the amount of grain boundaries, acting as the barrier for charge carrier mobility, results in the decrease of conductivity in the system.

8. Conclusions

Exploration related to the use of natural materials for functional materials has been applied in this study. Natural iron sand with the dominant magnetite (Fe_3O_4) content has been successfully synthesized through the chemical coprecipitation method as a starting material for producing hematite (α-Fe_2O_3). α-Fe_2O_3 has been successfully used as the source of Fe^{3+} ions to synthesize calcium ferrite and bismuth ferrite nanoparticles. The calcium ferrite powders synthesized by the chemical dissolved technique produce nano-sized crystals with the dominant phases of $CaFe_4O_7$ and $Ca_4Fe_{14}O_{25}$. The calcium ferrite powder has soft magnetic properties at room temperature which is attributed to the presence of dominant ferromagnetic phase and also oxygen vacancy in the nanoparticles. Magnetic parameters, such as saturation magnetic, are comparable to the barium-calcium hexaferrites, so that these nanoparticles have the potential application as microwave-absorbing materials. The bismuth ferrite powder, synthesized by the sol-gel method, exhibits multiferroic properties. The undoped $BiFeO_3$ possesses a weak ferromagnetism at room temperature. The magnetic parameters can be enhanced by Ni doping in the form of $BiFe_{0.9}Ni_{0.1}O_3$ nanoparticles. On the other hand, the electrical properties, i.e., dielectric constant, permittivity, and electrical conductivity, can be improved by Pb doping in the nanoparticles of $Bi_{0.9}Pb_{0.1}FeO_3$. The multiferroic behaviors

are strongly determined by the nano-sized effects, the presence of oxygen vacancies and impurities, and also the doping type affecting the phase stability in the perovskite structure of $BiFeO_3$ crystals. Considering the importance of applying these ferrite-based nanoparticles, investigations for obtaining pure phases of the nanoparticles from natural resources are very important and need further study.

Acknowledgements

Conflict of interest

We state that the article is original and all authors are aware of its content and approve its submission. This article has not been published previously, and it is not under consideration for publication elsewhere. I confirm that there is no conflict of interest exists.

Author details

Malik Anjelh Baqiya[1], Retno Asih[1], Muhammad Ghufron[2], Mastuki[1], Dwi Yuli Retnowati[1], Triwikantoro[1] and Darminto[1*]

1 Department of Physics, Faculty of Science, Institut Teknologi Sepuluh Nopember, Surabaya, Indonesia

2 Department of Physics, Faculty of Mathematics and Natural Science, University of Brawijaya, Malang, Indonesia

*Address all correspondence to: darminto@physics.its.ac.id

IntechOpen

References

[1] Musyarofah, Lestari ND, Nurlaila R, Muwwaqor NF, Triwikantoro, Pratapa S. Synthesis of high-purity zircon, zirconia, and silica nanopowders from local zircon sand. Ceramics International. 2019;**45**(6):6639-6647. DOI: 10.1016/j.ceramint.2018.12.152

[2] Baqiya A, Munasir M, Zainuri M, Arifin Z, Mashuri M, Triwikantoro T, et al. Nanopowders produced from natural sources using the simple coprecipitation method. In: Bartul Z, Trenor J, editors. Advances in Nanotechnology. Vol. 20. New York: Nova Science Publisher; 2017. pp. 1-38

[3] Triwikantoro, Baqiya MA, Heriyanto T, Mashuri, Darminto D. Nano-coating of aluminum surface using Fe_3O_4-based magnetic fluids. Journal of Superconductivity and Novel Magnetism. 2017;**30**(2):555-560. DOI: 10.1007/s10948-016-3813-7

[4] Baqiya MA, Taufiq A, Sunaryono, Ayun K, Zainuri M, Pratapa S, et al. Spinel-structured nanoparticles for magnetic and mechanical applications. In: Magnetic Spinels-Synthesis, Properties and Applications. London: Intech Open; 2017. pp. 253-272

[5] Baqiya MA, Taufiq A, Sunaryono, Munaji, Sari PS, Dwihapsari Y, et al. Development of PVA/Fe_3O_4 as smart magnetic hydrogels for biomedical applications. In: Hydrogels. London: IntechOpen; 2018. pp. 159-178

[6] Dubey V, Kain V. Synthesis of magnetite by coprecipitation and sintering and its characterization. Materials and Manufacturing Processes. 2018;**33**(8):835-839. DOI: 10.1080/10426914.2017.1401720

[7] Lemine OM, Omri K, Zhang B, El Mir L, Sajieddine M, Alyamani A, et al. Sol-gel synthesis of 8nm magnetite (Fe_3O_4) nanoparticles and their magnetic properties. Superlattices and Microstructures. 2012;**52**(4):793-799. DOI: 10.1016/j.spmi.2012.07.009

[8] Lei W, Liu Y, Si X, Xu J, Du W, Yang J, et al. Synthesis and magnetic properties of octahedral Fe_3O_4 via a one-pot hydrothermal route. Physics Letters A. 2017;**381**(4):314-318. DOI: 10.1016/j.physleta.2016.09.018

[9] Wu JH, Ko SP, Liu HL, Jung M-H, Lee JH, Ju J-S, et al. Sub 5nm Fe_3O_4 nanocrystals via coprecipitation method. Colloids and Surfaces A: Physicochemical and Engineering Aspects. 2008;**313-314**:268-272. DOI: 10.1016/j.colsurfa.2007.04.108

[10] Lian S, Kang Z, Wang E, Jiang M, Hu C, Xu L. Convenient synthesis of single crystalline magnetic Fe_3O_4 nanorods. Solid State Communications. 2003;**127**(9):605-608. DOI: 10.1016/S0038-1098(03)00580-5

[11] Wei Y, Han B, Hu X, Lin Y, Wang X, Deng X. Synthesis of Fe_3O_4 nanoparticles and their magnetic properties. Procedia Engineering. 2012;**27**:632-637. DOI: 10.1016/j.proeng.2011.12.498

[12] Pan Y, Zeng W, Li L, Zhang Y, Dong Y, Ye K, et al. Surfactant assisted, one-step synthesis of Fe_3O_4 nanospheres and further modified Fe_3O_4/C with excellent lithium storage performance. Journal of Electroanalytical Chemistry. 2018;**810**:248-254. DOI: 10.1016/j.jelechem.2018.01.025

[13] Ramesh R, Rajalakshmi M, Muthamizhchelvan C, Ponnusamy S. Synthesis of Fe_3O_4 nanoflowers by one pot surfactant assisted hydrothermal method and its properties. Materials Letters. 2012;**70**:73-75. DOI: 10.1016/j.matlet.2011.11.085

[14] Arévalo P, Isasi J, Caballero AC, Marco JF, Martín-Hernández F. Magnetic and structural studies of Fe_3O_4 nanoparticles synthesized via coprecipitation and dispersed in different surfactants. Ceramics International. 2017;**43**(13):10333-10340. DOI: 10.1016/j.ceramint.2017.05.064

[15] Deepak FL, Bañobre-López M, Carbó-Argibay E, Cerqueira MF, Piñeiro-Redondo Y, Rivas J, et al. A systematic study of the structural and magnetic properties of Mn-, Co-, and Ni-doped colloidal magnetite nanoparticles. The Journal of Physical Chemistry C. 2015;**119**(21):11947-11957. DOI: 10.1021/acs.jpcc.5b01575

[16] Pereira C, Pereira AM, Fernandes C, Rocha M, Mendes R, Fernández-García MP, et al. Superparamagnetic MFe_2O_4 (M = Fe, Co, Mn) nanoparticles: Tuning the particle size and magnetic properties through a novel one-step coprecipitation route. Chemistry of Materials. 2012;**24**(8):1496-1504. DOI: 10.1021/cm300301c

[17] Saha P, Rakshit R, Mandal K. Enhanced magnetic properties of Zn doped Fe_3O_4 nano hollow spheres for better bio-medical applications. Journal of Magnetism and Magnetic Materials. 2019;**475**:130-136. DOI: 10.1016/j.jmmm.2018.11.061

[18] Kandasamy G, Maity D. Recent advances in superparamagnetic iron oxide nanoparticles (SPIONs) for in vitro and in vivo cancer nanotheranostics. International Journal of Pharmaceutics. 2015;**496**(2):191-218. DOI: 10.1016/j.ijpharm.2015.10.058

[19] Zhu M, Wang Y, Meng D, Qin X, Diao G. Hydrothermal synthesis of hematite nanoparticles and their electrochemical properties. The Journal of Physical Chemistry C. 2012;**116**(30):16276-16285. DOI: 10.1021/jp304041m

[20] Lassoued A, Dkhil B, Gadri A, Ammar S. Control of the shape and size of iron oxide (α-Fe_2O_3) nanoparticles synthesized through the chemical precipitation method. Results in Physics. 2017;7:3007-3015. DOI: 10.1016/j.rinp.2017.07.066

[21] Tadic M, Panjan M, Damnjanovic V, Milosevic I. Magnetic properties of hematite (α-Fe_2O_3) nanoparticles prepared by hydrothermal synthesis method. Applied Surface Science. 2014;**320**:183-187. DOI: 10.1016/j.apsusc.2014.08.193

[22] Liu X, Chen K, Shim J-J, Huang J. Facile synthesis of porous Fe_2O_3 nanorods and their photocatalytic properties. Journal of Saudi Chemical Society. 2015;**19**(5):479-484. DOI: 10.1016/j.jscs.2015.06.009

[23] Kefeni KK, Msagati TAM, Nkambule TTI, Mamba BB. Synthesis and application of hematite nanoparticles for acid mine drainage treatment. Journal of Environmental Chemical Engineering. 2018;**6**(2):1865-1874. DOI: 10.1016/j.jece.2018.02.037

[24] Lagoeiro LE. Transformation of magnetite to hematite and its influence on the dissolution of iron oxide minerals. Journal of Metamorphic Geology. 1998;**16**(3):415-423. DOI: 10.1111/j.1525-1314.1998.00144.x

[25] Umar Saeed K, Abdul M, Nasrullah K, Amir M, Abdur R, Amanullah. Transformation mechanism of magnetite nanoparticles. Materials Science-Poland. 2015;**33**(2):278-285. DOI: 10.1515/msp-2015-0037

[26] Ding C, Lv X, Li G, Bai C, Xuan S, Tang K, et al. Reaction routes

of CaO–Fe_2O_3–TiO_2 and calcium ferrite–TiO_2 system in continuous heating process. In: 9th International Symposium on High-Temperature Metallurgical Processing. Cham, Heidelberg: Springer International Publishing; 2018. pp. 159-165

[27] Phillips B, Muan A. Phase equilibria in the system CaO-iron oxide in air and at 1 atm. O_2 pressure. Journal of the American Ceramic Society. 1958;**41**(11):445-454. DOI: 10.1111/j.1151-2916.1958.tb12893.x

[28] Boyanov BS. Solid state interactions in the systems $CaO(CaCO_3)$-Fe_2O_3 and $CuFe_2O_4$-CaO. Journal of Mining and Metallurgy Section B: Metallugy. 2005;**41**(B1):67-77

[29] Saleh HI. Synthesis and formation mechanisms of calcium ferrite compounds. Journal of Materials Science and Technology. 2004;**20**(5):530-534

[30] Gill N, Puthucheri S. Bandwidth enhancement of calcium ferrite-graphite nanocomposite microwave absorber using single square loop frequency selective surface. In: 11th International Conference on Industrial and Information Systems (ICIIS). 2016. pp. 827-832

[31] Sulaiman NH, Ghazali MJ, Majlis BY, Yunas J, Razali M. Superparamagnetic calcium ferrite nanoparticles synthesized using a simple sol-gel method for targeted drug delivery. Biomedical Materials and Engineering. 2015;**26**(1):103-110

[32] Asenath-Smith E, Lokuhewa IN, Misture ST, Edwards DD. p-type thermoelectric properties of the oxygen-deficient perovskite $Ca_2Fe_2O_5$ in the brownmillerite structure. Journal of Solid State Chemistry. 2010;**183**(7):1670-1677. DOI: 10.1016/j.jssc.2010.05.016

[33] Dhankhar S, Bhalerao G, Ganesamoorthy S, Baskar K, Singh S. Growth and comparison of single crystals and polycrystalline brownmillerite $Ca_2Fe_2O_5$. Journal of Crystal Growth. 2017;**468**:311-315. DOI: 10.1016/j.jcrysgro.2016.09.051

[34] Phan TL, Tho PT, Tran N, Kim DH, Lee BW, Yang DS, et al. Crystalline and electronic structures and magnetic and electrical properties of La-doped $Ca_2Fe_2O_5$ compounds. Journal of Electronic Materials. 2018;**47**(1):188-195. DOI: 10.1007/s11664-017-5841-x

[35] Jijil CP, Lokanathan M, Chithiravel S, Nayak C, Bhattacharyya D, Jha SN, et al. Nitrogen doping in oxygen-deficient $Ca_2Fe_2O_5$: A strategy for efficient oxygen reduction oxide catalysts. ACS Applied Materials & Interfaces. 2016;**8**(50):34387-34395. DOI: 10.1021/acsami.6b11718

[36] Martin LW, Schlom DG. Advanced synthesis techniques and routes to new single-phase multiferroics. Current Opinion in Solid State and Materials Science. 2012;**16**(5):199-215. DOI: 10.1016/j.cossms.2012.03.001

[37] Safi R, Shokrollahi H. Physics, chemistry and synthesis methods of nanostructured bismuth ferrite ($BiFeO_3$) as a ferroelectro-magnetic material. Progress in Solid State Chemistry. 2012;**40**(1):6-15. DOI: 10.1016/j.progsolidstchem.2012.03.001

[38] Čebela M, Zagorac D, Batalović K, Radaković J, Stojadinović B, Spasojević V, et al. $BiFeO_3$ perovskites: A multidisciplinary approach to multiferroics. Ceramics International. 2017;**43**(1):1256-1264. DOI: 10.1016/j.ceramint.2016.10.074

[39] Wang X, Yang C, Zhou D, Wang Z, Jin M. Chemical co-precipitation synthesis and properties of pure-phase $BiFeO_3$. Chemical Physics Letters.

2018;**713**:185-188. DOI: 10.1016/j.
cplett.2018.09.043

[40] Goldman AR, Fredricks JL, Estroff
LA. Exploring reaction pathways in the
hydrothermal growth of phase-pure
bismuth ferrites. Journal of Crystal
Growth. 2017;**468**:104-109. DOI:
10.1016/j.jcrysgro.2016.09.054

[41] Majid F, Mirza ST, Riaz S,
Naseem S. Sol-gel synthesis of $BiFeO_3$
nanoparticles. Materials Today:
Proceedings. 2015;**2**(10):5293-5297. DOI:
10.1016/j.matpr.2015.11.038

[42] Sankar Ganesh R, Sharma SK,
Sankar S, Divyapriya B, Durgadevi E,
Raji P, et al. Microstructure, structural,
optical and piezoelectric properties
of $BiFeO_3$ nanopowder synthesized
from sol-gel. Current Applied Physics.
2017;**17**(3):409-416. DOI: 10.1016/j.
cap.2016.12.008

[43] Wu H, Xue P, Lu Y, Zhu
X. Microstructural, optical and
magnetic characterizations of $BiFeO_3$
multiferroic nanoparticles synthesized
via a sol-gel process. Journal of Alloys
and Compounds. 2018;**731**:471-477.
DOI: 10.1016/j.jallcom.2017.10.087

[44] Wang L, Xu J-B, Gao B, Bian
L, Chen X-Y. Synthesis of pure
phase $BiFeO_3$ powders by direct
thermal decomposition of metal
nitrates. Ceramics International.
2013;**39**:221-225. DOI: 10.1016/j.
ceramint.2012.10.066

[45] Wang L, Xu J-B, Gao B, Chang
A-M, Chen J, Bian L, et al. Synthesis of
$BiFeO_3$ nanoparticles by a low-heating
temperature solid-state precursor
method. Materials Research Bulletin.
2013;**48**(2):383-388. DOI: 10.1016/j.
materresbull.2012.10.038

[46] Zheng S, Wang J, Zhang J, Ge
H, Chen Z, Gao Y. The structure and
magnetic properties of pure single phase

$BiFeO_3$ nanoparticles by microwave-
assisted sol-gel method. Journal of
Alloys and Compounds. 2018;**735**:945-
949. DOI: 10.1016/j.jallcom.2017.10.133

[47] Majid F, Riaz S, Tariq N, Naseem
S. Ferromagnetic behavior of undoped
$BiFeO_3$ thin films prepared by sol-
gel. Materials Today: Proceedings.
2015;**2**(10):5274-5279. DOI: 10.1016/j.
matpr.2015.11.035

[48] Betancourt-Cantera LG, Bolarín-
Miró AM, Cortés-Escobedo CA,
Hernández-Cruz LE, Sánchez-De
Jesús F. Structural transitions and
multiferroic properties of high
Ni-doped $BiFeO_3$. Journal of Magnetism
and Magnetic Materials. 2018;**456**:381-
389. DOI: 10.1016/j.jmmm.2018.02.065

[49] Chauhan S, Kumar M, Chhoker
S, Katyal SC, Singh H, Jewariya M,
et al. Multiferroic, magnetoelectric
and optical properties of Mn doped
$BiFeO_3$ nanoparticles. Solid State
Communications. 2012;**152**(6):525-529.
DOI: 10.1016/j.ssc.2011.12.037

[50] Costa LV, Deus RC, Foschini
CR, Longo E, Cilense M, Simões
AZ. Experimental evidence of enhanced
ferroelectricity in Ca doped $BiFeO_3$.
Materials Chemistry and Physics.
2014;**144**(3):476-483. DOI: 10.1016/j.
matchemphys.2014.01.022

[51] Dhir G, Uniyal P, Verma NK.
Multiferroic properties of Sr-doped
$BiFeO_3$ nanoparticles. Physica B:
Condensed Matter. 2018;**531**:51-57. DOI:
10.1016/j.physb.2017.12.004

[52] Tian Y, Xue F, Fu Q, Zhou L,
Wang C, Gou H, et al. Structural and
physical properties of Ti-doped $BiFeO_3$
nanoceramics. Ceramics International.
2018;**44**(4):4287-4291. DOI: 10.1016/j.
ceramint.2017.12.013

[53] Wang Y, Guo Z, Jia Q, Dong J,
Zhang J, Chen D. Effect of Nd/Mn

substitution on the structure and magnetic properties of nano-$BiFeO_3$. Journal of Alloys and Compounds. 2019;**786**:385-393. DOI: 10.1016/j.jallcom.2019.01.369

[54] Yuan X, Shi L, Zhao J, Zhou S, Li Y, Xie C, et al. Sr and Pb co-doping effect on the crystal structure, dielectric and magnetic properties of $BiFeO_3$ multiferroic compounds. Journal of Alloys and Compounds. 2017;**708**:93-98. DOI: 10.1016/j.jallcom.2017.02.288

[55] Asih R, Gufron M, Darminto. Synthesis of (Pb,Ni)-doped $BiFeO_3$ multiferroic systems via a sol-gel method and their magneto-electric properties. AIP Conference Proceedings. 2013;**1554**(1):50-53. DOI: 10.1063/1.4820281

[56] Asih R, Gufron M, Amrillah T, Arifani M, Hariyanto, Fitriyah N, et al. Effect of Pb doping on multiphase coexistence and magneto-electric properties of bismuth ferrite. AIP Conference Proceedings. 2014;**1617**(1):26-29. DOI: 10.1063/1.4897096

[57] Shokrollahi H. Magnetic, electrical and structural characterization of $BiFeO_3$ nanoparticles synthesized by co-precipitation. Powder Technology. 2013;**235**:953-958. DOI: 10.1016/j.powtec.2012.12.008

[58] Abushad M, Khan W, Naseem S, Husain S, Nadeem M, Ansari A. Influence of Mn doping on microstructure, optical, dielectric and magnetic properties of $BiFeO_3$ nanoceramics synthesized via sol-gel method. Ceramics International. 2019;**45**(6):7437-7445. DOI: 10.1016/j.ceramint.2019.01.035

[59] Costa LV, Rocha LS, Cortés JA, Ramirez MA, Longo E, Simões AZ. Enhancement of ferromagnetic and ferroelectric properties in

calcium doped $BiFeO_3$ by chemical synthesis. Ceramics International. 2015;**41**(8):9265-9275. DOI: 10.1016/j.ceramint.2015.03.086

[60] Liu H, Pu Y, Shi X, Yuan Q. Dielectric and ferroelectric properties of $BiFeO_3$ ceramics sintered in different atmospheres. Ceramics International. 2013;**39**:S217-S220. DOI: 10.1016/j.ceramint.2012.10.065

[61] Arifin Z, Riyanto A, Lailiyah Q, Triwikantoro, Pratapa S, Darminto. Precipitated $CaCO_3$ with unique crystalline morphology prepared from limestone. Transactions of the Indian Ceramic Society. 2015;**74**(4):202-207. DOI: 10.1080/0371750X.2015.1084892

[62] Lutterotti L, Scardi P. Simultaneous structure and size-strain refinement by the Rietveld method. Journal of Applied Crystallography. 1990;**23**(4):246-252. DOI: 10.1107/S0021889890002382

[63] Rietveld H. A profile refinement method for nuclear and magnetic structures. Journal of Applied Crystallography. 1969;**2**(2):65-71. DOI: 10.1107/S0021889869006558

[64] Hughes H, Roos P, Goldring DC. X-ray data on some calcium-iron-oxygen compounds. Mineralogical Magazine and Journal of the Mineralogical Society. 2018;**36**(278):280-291. DOI: 10.1180/minmag.1967.036.278.10

[65] Tsuyuki N, Koizumi K, Umemura Y. Surface structure of converter slag stabilized by heating. Journal of the American Ceramic Society. 2007;**90**(1):225-229. DOI: 10.1111/j.1551-2916.2006.01344.x

[66] Ding C, Lv X, Chen Y, Bai C. Crystallization kinetics of $2CaO \cdot Fe_2O_3$ and $CaO \cdot Fe_2O_3$ in the $CaO–Fe_2O_3$ system. ISIJ International.

2016;**56**(7):1157-1163. DOI: 10.2355/
isijinternational.ISIJINT-2015-710

[67] Millon E, Malaman B, Bonazebi
A, Brice JF, Gerardin R, Evrard
O. Structure cristalline du ferrite
hemicalcique $CaFe_4O_7$. Materials
Research Bulletin. 1986;**21**(8):985-994.
DOI: 10.1016/0025-5408(86)90136-4

[68] Gerardin R, Millon E,
Bonazebi A, Brice JF, Jeannot F,
Evrard O. Structures et proprietes
magnetiques des ferrites de calcium
pseudo hexagonaux $Ca_4Fe_9O_{17}$,
$CaFe_4O_7$ et $Ca_3Fe_{15}O_{25}$. Journal
of Physics and Chemistry of
Solids. 1988;**49**(4):343-348. DOI:
10.1016/0022-3697(88)90090-X

[69] Jotania RB, Khomane RB,
Chauhan CC, Menon SK, Kulkarni
BD. Synthesis and magnetic properties
of barium–calcium hexaferrite
particles prepared by sol-gel and
microemulsion techniques. Journal
of Magnetism and Magnetic Materials.
2008;**320**(6):1095-1101. DOI: 10.1016/j.
jmmm.2007.10.032

[70] Samariya A, Dolia SN, Prasad
AS, Sharma PK, Pareek SP, Dhawan
MS, et al. Size dependent structural
and magnetic behaviour of
$CaFe_2O_4$. Current Applied Physics.
2013;**13**(5):830-835. DOI: 10.1016/j.
cap.2012.12.009

[71] Ke H, Wang W, Wang Y, Xu J,
Jia D, Lu Z, et al. Factors controlling
pure-phase multiferroic $BiFeO_3$
powders synthesized by chemical
co-precipitation. Journal of Alloys and
Compounds. 2011;**509**(5):2192-2197.
DOI: 10.1016/j.jallcom.2010.09.213

[72] Xu J-H, Ke H, Jia D-C, Wang W,
Zhou Y. Low-temperature synthesis
of $BiFeO_3$ nanopowders via a sol-
gel method. Journal of Alloys and
Compounds. 2009;**472**(1):473-477. DOI:
10.1016/j.jallcom.2008.04.090

[73] Carvalho TT, Tavares PB. Synthesis
and thermodynamic stability of
multiferroic $BiFeO_3$. Materials Letters.
2008;**62**(24):3984-3986. DOI: 10.1016/j.
matlet.2008.05.051

[74] Sakar M, Balakumar S, Saravanan
P, Jaisankar SN. Annealing temperature
mediated physical properties of
bismuth ferrite ($BiFeO_3$) nanostructures
synthesized by a novel wet chemical
method. Materials Research Bulletin.
2013;**48**(8):2878-2885. DOI: 10.1016/j.
materresbull.2013.04.008

[75] Yang N, Yang H, Jia J, Pang
X. Formation and magnetic properties
of nanosized $PbFe_{12}O_{19}$ particles
synthesized by citrate precursor
technique. Journal of Alloys and
Compounds. 2007;**438**(1):263-267. DOI:
10.1016/j.jallcom.2006.08.037

[76] Zhu XH, Defaÿ E, Lee Y, André B,
Aïd M, Zhu JL, et al. High permittivity
$Bi_{24}Fe_2O_{39}$ thin films prepared by a low
temperature process. Applied Physics
Letters. 2010;**97**(23):232903. DOI:
10.1063/1.3524492

[77] Sun L, Zhang R, Wang Z, Ju L,
Cao E, Zhang Y. Structural, dielectric
and magnetic properties of $NiFe_2O_4$
prepared via sol-gel auto-combustion
method. Journal of Magnetism and
Magnetic Materials. 2017;**421**:65-70.
DOI: 10.1016/j.jmmm.2016.08.003

[78] Pradhan AK, Zhang K,
Hunter D, Dadson JB, Loiutts GB,
Bhattacharya P, et al. Magnetic and
electrical properties of single-phase
multiferroic $BiFeO_3$. Journal of Applied
Physics. 2005;**97**(9):093903. DOI:
10.1063/1.1881775

[79] Jia D-C, Xu J-H, Ke H, Wang W,
Zhou Y. Structure and multiferroic
properties of $BiFeO_3$ powders. Journal
of the European Ceramic Society.
2009;**29**(14):3099-3103. DOI: 10.1016/j.
jeurceramsoc.2009.04.023

[80] Ederer C, Spaldin NA. Weak ferromagnetism and magnetoelectric coupling in bismuth ferrite. Physical Review B. 2005;**71**(6):060401. DOI: 10.1103/PhysRevB.71.060401

[81] Jaffari GH, Aftab M, Samad A, Mumtaz F, Awan MS, Shah SI. Effects of dopant induced defects on structural, multiferroic and optical properties of $Bi_{1-x}Pb_xFeO_3$ ($0 \leq x \leq 0.3$) ceramics. Materials Research Express. 2018;**5**(1):016103. DOI: 10.1088/2053-1591/aaa14f

[82] Makhdoom AR, Akhtar MJ, Rafiq MA, Siddique M, Iqbal M, Hasan MM. Enhancement in the multiferroic properties of $BiFeO_3$ by charge compensated aliovalent substitution of Ba and Nb. AIP Advances. 2014;**4**(3):037113. DOI: 10.1063/1.4869081

[83] Khomchenko VA, Kiselev DA, Kopcewicz M, Maglione M, Shvartsman VV, Borisov P, et al. Doping strategies for increased performance in $BiFeO_3$. Journal of Magnetism and Magnetic Materials. 2009;**321**(11):1692-1698. DOI: 10.1016/j.jmmm.2009.02.008

[84] Verma KC, Kotnala RK. Tailoring the multiferroic behavior in $BiFeO_3$ nanostructures by Pb doping. RSC Advances. 2016;**6**(62):57727-57738. DOI: 10.1039/C6RA12949H

[85] Ederer C, Spaldin NA. Influence of strain and oxygen vacancies on the magnetoelectric properties of multiferroic bismuth ferrite. Physical Review B. 2005;**71**(22):224103. DOI: 10.1103/PhysRevB.71.224103

[86] Khomchenko VA, Kiselev DA, Selezneva EK, Vieira JM, Lopes AML, Pogorelov YG, et al. Weak ferromagnetism in diamagnetically-doped $Bi_{1-x}A_xFeO_3$ (A = Ca, Sr, Pb, Ba) multiferroics. Materials Letters.

2008;**62**(12):1927-1929. DOI: 10.1016/j.matlet.2007.10.044

[87] Hwang JS, Yoo YJ, Lee YP, Kang J-H, Lee KH, Lee BW, et al. Reinforced magnetic properties of Ni-doped $BiFeO_3$ ceramic. Journal of the Korean Physical Society. 2016;**69**(3):282-285. DOI: 10.3938/jkps.69.282

[88] Zhao J, Zhang X, Liu S, Zhang W, Liu Z. Effect of Ni substitution on the crystal structure and magnetic properties of $BiFeO_3$. Journal of Alloys and Compounds. 2013;**557**:120-123. DOI: 10.1016/j.jallcom.2013.01.005

[89] Ederer C, Spaldin NA. Recent progress in first-principles studies of magnetoelectric multiferroics. Current Opinion in Solid State and Materials Science. 2005;**9**(3):128-139. DOI: 10.1016/j.cossms.2006.03.001

[90] Mazumder R, Sen A. Effect of Pb-doping on dielectric properties of $BiFeO_3$ ceramics. Journal of Alloys and Compounds. 2009;**475**(1):577-580. DOI: 10.1016/j.jallcom.2008.07.082

[91] Chaigneau J, Haumont R, Kiat JM. Ferroelectric order stability in the $Bi_{1-x}Pb_xFeO_3$ solid solution. Physical Review B. 2009;**80**(18):184107. DOI: 10.1103/PhysRevB.80.184107

[92] Zhang X, Sui Y, Wang X, Tang J, Su W. Influence of diamagnetic Pb doping on the crystal structure and multiferroic properties of the $BiFeO_3$ perovskite. Journal of Applied Physics. 2009;**105**(7):07D918. DOI: 10.1063/1.3079770

[93] Kianinia M, Ahadi K, Nemati A. Investigation of dark and light conductivities in calcium doped bismuth ferrite thin films. Materials Letters. 2011;**65**(19):3086-3088. DOI: 10.1016/j.matlet.2011.06.052

[94] Kumar A, Sharma P, Yang W, Shen J, Varshney D, Li Q. Effect of La and Ni substitution on structure, dielectric and ferroelectric properties of $BiFeO_3$ ceramics. Ceramics International. 2016;**42**(13):14805-14812. DOI: 10.1016/j.ceramint.2016.06.113

[95] Nadeem M, Khan W, Khan S, Husain S, Ansari A. Tailoring dielectric properties and multiferroic behavior of nanocrystalline $BiFeO_3$ via Ni doping. Journal of Applied Physics. 2018;**124**(16):164105. DOI: 10.1063/1.5050946